JCTC Journal of Chemical Theory and Computation

Temperature Dependence of Protein Dynamics Simulated with Three Different Water Models

Dennis C. Glass,[†] Marimuthu Krishnan,[†] David R. Nutt,[‡] and Jeremy C. Smith*,[†]

University of Tennessee/ORNL Center for Molecular Biophysics, Oak Ridge National Laboratory, 1 Bethel Valley Road, Oak Ridge, Tennessee 37831, and Department of Chemistry, University of Reading, Whiteknights, Reading RG6 6AD, United Kingdom

Received December 3, 2009

Abstract: The effect of variation of the water model on the temperature dependence of protein and hydration water dynamics is examined by performing molecular dynamics simulations of myoglobin with the TIP3P, TIP4P, and TIP5P water models and the CHARMM protein force field at temperatures between 20 and 300 K. The atomic mean-square displacements, solvent reorientational relaxation times, pair angular correlations between surface water molecules, and time-averaged structures of the protein are all found to be similar, and the protein dynamical transition is described almost indistinguishably for the three water potentials. The results provide evidence that for some purposes changing the water model in protein simulations without a loss of accuracy may be possible.

1. Introduction

Water plays an important role in many chemical and biological processes.[1−9] For example, hydration water strongly influences the three-dimensional structure, dynamics, and function of proteins.[2] Water−protein interactions modify the free energy landscape that determines the folding, structure, and stability of proteins.[3−5] Internal protein dynamics, which are required for biological functions, are dependent on the level of hydration,[6] and dynamical coupling between the protein and water influences conformational flexibility.[7−10]

Protein hydration water can be grouped into two classes: internal water molecules, which can play structural and/or catalytic roles,[11,12] and external surface water molecules. Hydration water is experimentally estimated to account for 10−15% of the total cell water,[13,14] of which a small fraction of ∼0.1% is internal water molecules. Properties of water in the external hydration shell are modified compared to the bulk, with, for example, changes in average density[15−17] and perturbations in translational and rotational dynamics, and these changes have been extensively investigated using techniques such as neutron scattering,[13,18−25] nuclear magnetic resonance,[26−31] fluorescence spectroscopy,[32] mid-infrared pump−probe spectroscopy,[33] and molecular dynamics (MD) simulations.[21,33−40]

Empirical, molecular mechanics force fields, such as CHARMM,[41−43] AMBER,[44] GROMOS,[45] and OPLS-AA[46] are widely employed in atomistic MD simulations of biological molecules and, in order to represent the protein−solvent energy accurately, most molecular simulation applications employ explicit water models. A large number of water models is available. However, individual biomolecular force fields have normally been parametrized for use with a single water model (see e.g. ref 47) such that, during the parametrization, care can be taken to correctly balance water−water, water−protein, and protein−protein interactions. Nevertheless, the question arises as to whether the water−protein potentials are sufficiently robust so that alternative water models may be employed with any given biomolecular force field without a serious loss of accuracy. Flexibility in the choice of the water model may be of particular interest when the system is to be simulated at nonphysiological temperatures or pressures, as required, for example, in studies on antifreeze proteins,[48,49] under which circumstances different water models may exhibit significantly different properties (see e.g., ref 50), and/or when water properties are specifically under investigation for which an alternative water potential may be more accurate than the original. As another example, the dynamical equilibrium

* Corresponding author e-mail: smithjc@ornl.gov.
[†] Oak Ridge National Laboratory.
[‡] University of Reading.

10.1021/ct9006508
Published on Web 03/04/2010

between water molecules on the protein surface and bulk is important in the study of the dielectric relaxation of aqueous protein solutions, and the rate of transition of water molecules from bulk to interface or vice versa is influenced by the choice of water model.[51] The need for alternate water models to better characterize the hydrophobic effect,[52] spectral properties,[53] solvation free energies,[54] and hydration dynamics[55,56] of proteins has also been discussed.

In recent work, the effects of varying the water model in molecular mechanics and dynamics calculations on the hydration of N-methylacetamide (NMA) and other small solute molecules and a small protein using the CHARMM force field[41−43] were examined with a focus on structural aspects, e.g., distribution functions around different biomolecular sites.[57] The overall description of solvation and biomolecular properties were found to be similar for the three models tested: TIP3P, TIP4P, and TIP5P.[50,58] The CHARMM protein force field was originally parametrized for use with the TIP3P potential. However, the results provide an indication that molecular simulations with the CHARMM force field may in some cases be performed with water models other than TIP3P.

In the present work, we compare the results of using the above three water models (TIP3P, 4P, 5P) on the temperature dependence of internal protein motion. Experimental and theoretical studies have found that proteins undergo a transition in internal dynamics at $T_g \approx 180-220$ K,[59−70] characterized by a rapid increase in the average protein atomic mean-square displacement above T_g. The transition at T_g is strongly coupled to the solvent dynamics.[2,67−69,71−81] An additional low-temperature transition (~150 K), that has been attributed to the activation of methyl group rotations, is present also in dehydrated proteins.[71,82−86] The dynamical transition at T_g can be eliminated when dehydrating the protein or coating it with a bioprotectant,[87] and the value of T_g can be shifted by changing the solvent composition.[88] MD simulations have demonstrated that the T_g dynamical transition is driven by translational solvent dynamics.[68,89] For some proteins, the T_g dynamical transition has also been correlated with protein activity,[64,66,73,90,91] although activity has also been observed for $T < T_g$.[92−95]

The question arises as to whether the dynamical properties of the protein are affected by the choice of the water model used. To investigate this, we have performed simulations of myoglobin at temperatures ranging from 20 to 300 K using the TIP3P, TIP4P, or TIP5P potentials and the CHARMM protein force field.[41−43] The protein dynamical transition was found to be unaffected by changes in the solvent model. Moreover, although the bulk properties of the three water models are markedly different, when interacting with the protein surface, the three water models behave similarly.

2. Methods

The set of models considered here is the TIP3P, TIP4P, and TIP5P family.[50,58] TIP3P is the standard model in the widely used CHARMM force fields. However, TIP4P and TIP5P are easy to implement for use with CHARMM and exhibit improved bulk water properties, as described below.

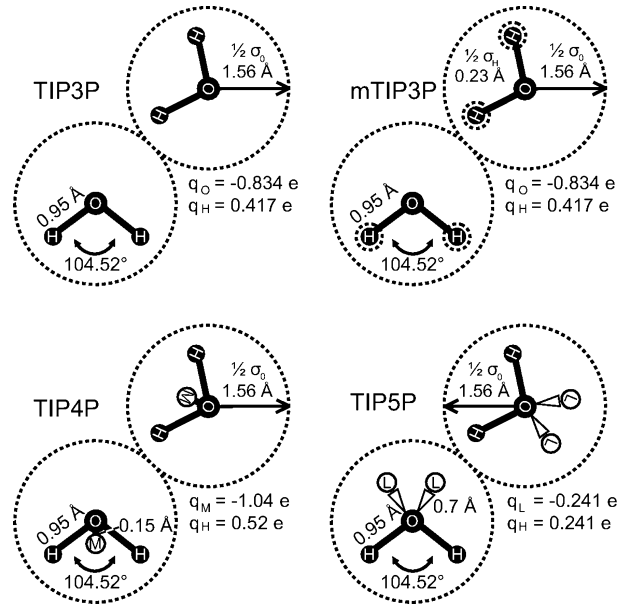

Figure 1. TIPnP geometries. Dashed lines represent 1/2 of the van der Waals radius σ_0.

Table 1. TIP3P, TIP4P, TIP5P, and mTIP3P Potential Energy Parameters

	TIP3P	mTIP3P	TIP4P	TIP5P
q_H	0.417	0.417	0.520	0.241
q_O	−0.834	−0.834		
q_M			−1.040	
q_L			−0.241	
σ_{OO}/A	3.5364	3.5364	3.5399	3.5021
ε_O/kcal/mol	0.1521	0.1521	0.1550	0.1600
σ_{HH}/A		0.4490		
ε_H/kcal/mol		0.0460		
r_{OH}/A	0.9572	0.9572	0.9572	0.9572
r_{OM}/A			0.15	
r_{OL}/A				0.7
θ_{HOH}/deg	104.52	104.52	104.52	104.52
θ_{LOL}/deg				109.47

The TIP geometries and associated parameters are shown in Figure 1 and Table 1. In the TIP3P model, charges are placed at the hydrogen positions and on the oxygen, resulting in three interaction sites. A van der Waals term provides additional nonbonding interactions involving the oxygen atoms only.[58] Geometrical parameters were assigned according to experimental gas phase values.

mTIP3P is a slightly modified version of TIP3P, commonly used with CHARMM,[41−43] and includes additional van der Waals interaction sites at the hydrogen positions.[96] The effect of these additional terms on the properties of TIP3P has been shown to be small.[97] Therefore, in the following, TIP3P is used to refer to the CHARMM-modified version, mTIP3P.

The combination of TIP3P with the CHARMM force field has proven to be useful for examining the structure and dynamics of biomolecular systems. However, although TIP3P adequately describes the first hydration shell of bulk water, it lacks accuracy for the second hydration shell, for which the corresponding peak in the oxygen−oxygen radial distribution function is almost completely absent.[50] TIP4P, in which the oxygen charge site is moved along the HOH

bisector toward the molecular center of mass, better reproduces experimental distribution functions than TIP3P.[58] In TIP5P, there are two lone-pair interaction sites, L, moved from the oxygen along the HOH bisector away from the hydrogens and symmetrically placed out of the HOH plane with $\angle_{LOL} = 109.47°$.[50] The TIP4P and TIP5P oxygens carry no charge. TIP5P, explicitly incorporating tetrahedrality in the water model, is especially successful in reproducing bulk water density over a wide range of temperatures.[50]

Here, the CHARMM program package version c33b2 was used to perform MD simulations of hydrated myoglobin with the CHARMM22 force field and TIP3P, TIP4P, or TIP5P water.[41−43] The protein−water heteroatomic interaction parameters were calculated using the standard Lorentz−Berthelot mixing rule, which is defined as follows:

$$\sigma_{PW} = \frac{\sigma_P + \sigma_W}{2}; \varepsilon_{PW} = \sqrt{\varepsilon_P \varepsilon_W}$$

where (σ_P, ε_P) and (σ_W, ε_W) correspond to Lennard-Jones parameters associated with protein and water atoms, respectively. The 1.15 Å resolution myoglobin structure 1A6G, taken from the RCSB Protein Data Bank (www.pdb.org),[98] was used as the starting protein configuration. The model was constructed as in ref 68 to mimic a hydrated powder sample and thus model the experimental neutron scattering setup of ref 77, the data from which serve as a reference here. To do this, the protein was solvated by placing it in a box of water, retaining only those 492 molecules closest to the protein. The temperature dependent dynamical properties in the present simulations were found to be very similar to those derived from NPT simulations in solution on the same myoglobin structure.[86]

Electrostatic interactions were truncated using a shift function with a 12 Å cutoff, and a switch function was used for the truncation of van der Waals interactions between 10 and 12 Å. The SHAKE algorithm was used to constrain all bond lengths involving hydrogens.[99] The structures were energy minimized using 600 steepest descent steps and 2500 conjugate gradient steps with the protein atoms fixed, then with fixed solvent allowing the protein to move, and finally without any constraints.

After heating to the desired temperature in steps of 5 K every 1000 dynamics steps, the system was equilibrated for 400 ps. Subsequently, 1 ns production runs were performed in the NVT ensemble at temperatures from 20 to 300 K in intervals of 20 K and in smaller intervals of 10 K between 120 and 240 K. The system was kept at constant temperature using the weak coupling algorithm of ref 100. A time step of 1 fs was used for the integration of the equations of motion. Coordinates and velocities were saved every 50 steps. The simulation protocol was the same for all temperatures and water models.

In order to examine in more detail the influence of the water model on the time averaged protein structure at 300 K, 10 additional simulations of 1 ns length were performed for each water model, starting with different, randomly chosen, initial velocity assignments.

To avoid potential artifacts, no restraining potential was applied to the water molecules to prevent evaporation. Subsequently, for $T > 260$ K, a small number of molecules evaporated from the water shell surrounding the protein, and these were excluded from all analyses. No evaporation occurred for $T < 260$ K, including during extended 7 ns simulations with TIP3P at 180, 220, and 260 K.

In addition to the above calculations, for comparison purposes, simulations of bulk water using the TIP water models were performed. For these, GROMACS 4.0[101] was used to generate a 30 Å cubic water box at 300 K and 1 atm pressure containing 895 molecules for TIP3P, 886 for TIP4P, and 878 for TIP5P. The electrostatic interactions were treated in the same way as for the above protein simulations, and periodic boundary conditions were applied. The configurations were energy minimized using 600 steepest descent steps, equilibrated for 500 ps at the desired temperatures and, subsequently, 1 ns production runs were performed in the NVT ensemble at temperatures from 20 to 300 K in intervals of 20 K and in smaller intervals of 10 K between 100 and 260 K. The system was kept at a constant temperature using the weak coupling algorithm of ref 100. A time step of 2 fs was used. Coordinates were saved every 50 steps. The simulation protocol was again the same for all temperatures and water models.

Additional MD simulations of myoglobin fully solvated in a periodic TIP3P water box ($68 \times 68 \times 52$ Å^3 dimensions) were carried out using the NAMD software.[102] The Particle Mesh Ewald (PME) method was used for the electrostatics, and a switch function was used for truncation of van der Waals interactions between 10 and 12 Å. The starting configurations were energy minimized using 6000 conjugate gradient steps followed by 1 ns equilibration and 1 ns production runs in the NPT ensemble. The equations of motion were integrated with a time step of 1 fs, and the atomic coordinates were saved at every 100 fs. Using the Langevin thermostat and barostat, simulations were carried out at a range of temperatures between 20 and 300 K and at 1 atm of pressure. The temperature dependence of the Kirkwood g-factor determined from this set of simulations serves for comparison with results obtained from the hydrated powder model.

3. Results

3.1. Time-Averaged Structures. The influence of the water models on the average structure of myoglobin is first investigated. The time-averaged structures were calculated for all 30 independent simulations at 300 K and were compared using a root-mean-square deviation (RMSD) per residue, defined here as

$$\mathrm{RMSD}_i^{A,B} = \sqrt{\frac{\sum_{j=1}^{N_i} (x_j^A - x_j^B)^2}{N_i}} \quad (1)$$

where i is the residue number, N_i is the number of protein heavy atoms in residue i, A and B are any two given time-averaged structures, and $x_j^{A/B}$ denotes the heavy atom coordinates. Convergence was checked by comparing RMSD values from the first and second half of each simulation, which were found to be in close agreement.

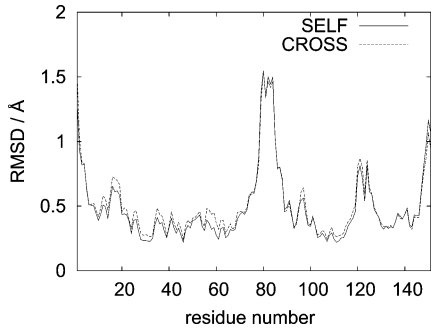

Figure 2. Backbone heavy-atom RMSD per residue at 300 K. Average over pairs of structures solvated in the same or in different water models. "SELF" refers to RMSD values between protein structures solvated by the same water model, whereas "CROSS" refers to deviations in configurations between the models.

Figure 2 shows the backbone heavy-atom RMSD per residue based on the average over all pairs (A,B) of structures solvated in the same or in different water models. "SELF" refers to RMSD values between protein structures solvated by the same water model, whereas "CROSS" refers to deviations in configurations between the models, for example, structures of the protein in TIP3P compared with structures in TIP4P or TIP5P.

Neglecting the five C- and N-terminal residues, the $\mathrm{RMSD}_i^{A,B}$ averaged over residues is 0.47 ± 0.25 Å, averaged over "SELF" is 0.46 ± 0.26 Å, and averaged over "CROSS" is 0.49 ± 0.25 Å, and the average difference between "SELF" and "CROSS" is 0.035 ± 0.026 Å. Therefore, the RMSD per residue is similar for both the "SELF" and "CROSS" data sets, indicating that variation of the water model does not significantly influence the time-averaged protein RMSD.

3.2. Mean-Square Displacement. The mean-square displacement $\langle r^2(t)\rangle$ is defined as

$$\langle r^2(t)\rangle = \left\langle \frac{1}{N}\sum_{i=0}^{N} (r_i(t + t_0) - r_i(t_0))^2 \right\rangle_{i,t_0} \qquad (2)$$

where N is the number of atoms, $(r_i(t + t_0) - r_i(t_0))$ is the displacement of atom i in time t, and $\langle\cdot\rangle_{i,t_0}$ represents the ensemble average, approximated as a time average over t_0 by assuming ergodicity.

The mean-square displacement (MSD) averaged over the heavy atoms of myoglobin was calculated for all temperatures and water models. Figure 3C shows the time evolution of heavy atom MSD of myoglobin at various temperatures, while Figure 3A exhibits time-averaged MSD as a function of temperaure. The inset in Figure 3 A shows an expanded view of the low-temperature region, up to $T \approx 210$ K. The MSD rises linearly for low temperatures until a first change in the gradient at $T \approx 150$ K, which has been attributed to the activation of methyl group rotations.[71,84,86] At $T \approx 220$ K, $\langle r^2(t)\rangle$ exhibits a further increase in gradient corresponding to the solvent-driven dynamical transition. $\langle r^2(t)\rangle$, both for <220 K and >220 K, is similar using all three TIP water models.

Figure 3B shows the $\langle r^2(t)\rangle$ of the water molecules in the protein simulations as a function of temperature. The insets

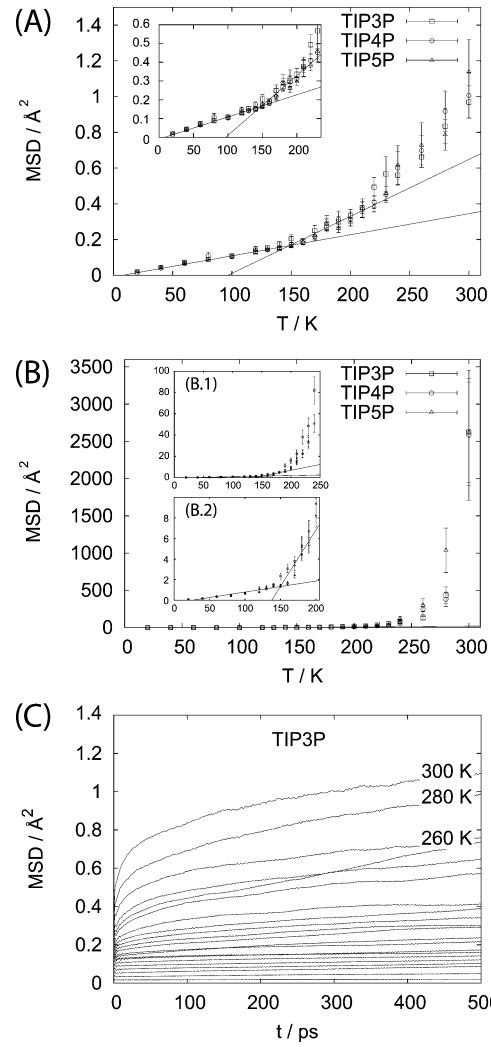

Figure 3. (A) Heavy atom mean-square displacement of myoglobin solvated in TIP3P, TIP4P, or TIP5P as a function of temperature. The inset shows an expanded view of the low temperature region up to $T \approx 210$ K. (B) Mean-square displacement of the hydration shell water as a function of temperature. The insets (B.1 and B.2) give expanded views since the data cover multiple orders of magnitude. (C) Time dependent mean-square displacement of myoglobin in TIP3P as a function of time at different temperatures.

B.1 and B.2 give expanded views since the data cover multiple orders of magnitude. The profiles qualitatively resemble Figure 3A; i.e., the MSD for the water molecules rises linearly for low temperatures until, interestingly, a first change in slope is seen at $T \approx 150$ K (Figure 3B.2) followed by a second transition at $T \approx 200$ K (Figure 3B.1).

The transition at 220 K in the protein has been previously observed and the strong coupling between the solvent and protein characterized.[62,65,68,73,76,78,80,89,103−109] However, the low-T transition at 150 K for water was unexpected, and the question therefore arises as to whether it would occur independent of the protein. To check this, a set of simulations of pure TIP water was performed, as described in the Methods. Figure 4A shows the TIP water mean-square displacements as a function of temperature. A comparison between Figures 3B and 4A indicates that, while the dynamical transition behavior of the protein and protein

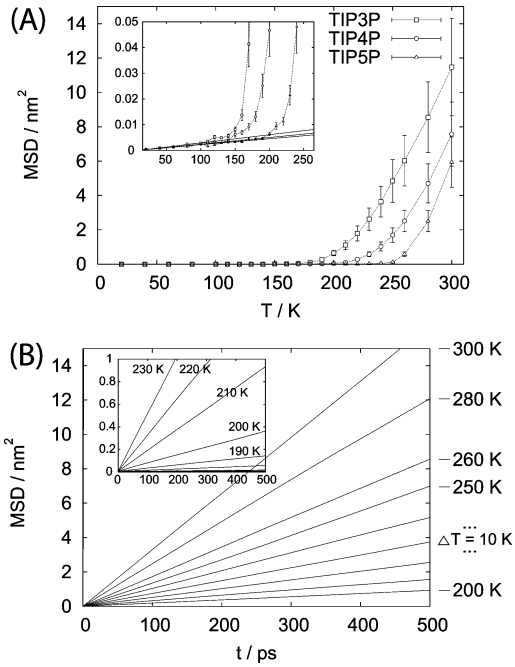

Figure 4. (A) Mean-square displacement of TIP3P, TIP4P, or TIP5P water molecules as a function of temperature from bulk water simulations. The inset shows an expanded view of the low temperature region. The solid lines corresponds to linear fits for $T = 20-100$ K. (B) Mean-square displacement as a function of time for TIP3P and various temperatures. The insets show data belonging to further temperatures in an appropriate magnification of the abscissa.

hydration water are similar, they do not resemble that of the bulk water models.

The data for the three TIP models exhibit similar properties in that $\langle r^2(t)\rangle$ is linear for $T \leq T_l$. However unlike in the solution simulations, the temperature at which the slope changes, T_l, is markedly different for the three models with $T_l \approx 120$ K for TIP3P, 140 K for TIP4P, and 190 K for TIP5P. Further, again unlike the data for the hydrated protein, the bulk data do not show two distinct changes in slope.

The self-diffusion constant, D, was calculated from the linear part of each mean-squared displacement, at, i.e., $t >$ 200 ps (see Figure 4B), using the Einstein relation:

$$\lim_{t\to\infty}\langle |r(t_0 + t) - r(t_0)|^2\rangle = 6Dt \tag{3}$$

where $r(t)$ is the position of the water oxygen atom and $\langle\cdot\rangle$ denotes averaging over both time origins t_0 and the water molecules. D, in units of 10^{-5} cm^2/s, at 300 K is found to be 5.46 ± 0.02 (TIP3P), 3.60 ± 0.06 (TIP4P), and 2.82 ± 0.02 (TIP5P). Corresponding values in the literature vary depending on the simulation setup, but reported values using a similar protocol to that used here (i.e., shift electrostatics) in the NPT ensemble are 5.8 ± 0.2 (TIP3P), 3.78 ± 0.02 (TIP4P), and 2.94 ± 0.06 (TIP5P),[110] in good agreement with the present work. For completeness, in Table 2, D is also given for the other temperatures.

3.3. Heterogeneous Distribution of Anharmonic Motions among Protein Residues. To quantify the fraction of protein residues that exhibit large anharmonic dynamics, the MSD per residue ($\langle r^2(t)\rangle_i$, where i denotes the residue index) was calculated. $\langle r^2(t)\rangle_i$ is decomposed into harmonic and anharmonic components as follows:

$$\langle r^2(t)\rangle_i = \langle r^2(t)\rangle_{i,\text{harmonic}} + \langle r^2(t)\rangle_{i,\text{anharmonic}} \tag{4}$$

where $\langle r^2(t)\rangle_{i,\text{harmonic}}$ is obtained by linearly fitting $\langle r^2(t)\rangle_i$ for $T \leq 140$ K and extrapolating to higher T.

A residue is denoted as exhibiting anharmonic dynamics if $\langle r^2(t)\rangle_i > (\langle r^2(t)\rangle_{i,\text{harmonic}} + 2\sigma)$, where σ is the standard deviation at the onset of anharmonicity (140 K). As a control, it was determined whether the onset of anharmonicity depends on the temperature interval chosen for the estimation of harmonic dynamics: using 20−100 K as the fitting interval and σ_{100K}, the procedure was found to give similar results.

Figure 5 shows the temperature dependence of the fraction of residues exhibiting anharmonic dynamics. For $T \leq 140$ K, almost all residues exhibit only harmonic motion, with $\langle r^2(t)\rangle_i$ similar to each other, while an abrupt change is evident at higher T, as an increasing fraction of residues exhibits anharmonic dynamics. Even well above the dynamical transition temperature at 260 K, approximately 25% of the residues still remain harmonic. This result is consistent with previous simulation work on myoglobin, in which the onset of anharmonicity was found to be gradual with T.[69] Again, when comparing the protein simulations using different water models, there are no statistically significant differences.

3.4. Reorientational Relaxation Time. The rotational dynamics of water can be characterized by the water dipole orientation autocorrelation function, $C(t)$:

$$C(t) = \langle \vec{e}_i(t + t_0)\cdot\vec{e}_i(t_0)\rangle_{i,t_0} \tag{5}$$

where $\vec{e}_i(t)$ is a unit vector along the water dipole. For liquids, $C(t)$ decays to zero as the dipole loses its memory of its initial orientation.

Since the structural and dynamic properties of the hydration layer water molecules depend on the heterogeneous surface roughness and charge distribution,[21,24,39,40,111] a multiexponential decay is expected. From the protein simulations, the reorientational relaxation time of water, τ, was calculated by fitting the following triple exponential function to $C(t)$:

$$\begin{aligned} C(t) = {} & a_0\exp(-t/\tau_0) + a_1\exp(-t/\tau_1) + \\ & (1 - a_0 - a_1)\exp(-t/\tau_2) \end{aligned} \tag{6}$$

Equation 6 was found to capture the decay in the target data, whereas the fitting procedure failed for simpler fitting functions. The relaxation time, τ, was derived using the following relation:

$$\tau = a_0\tau_0 + a_1\tau_1 + (1 - a_0 - a_1)\tau_2 \tag{7}$$

Figure 6A shows $C(t)$ together with the fit of eq 7 for TIP3P hydration water at different temperatures. $C(t)$'s for TIP4P and TIP5P hydration water exhibit similar decay behaviors (not shown). In general, the profiles consist of a fast decay on the picosecond time scale followed by slower dynamics. For most temperatures, $C(t)$ does not fully decay to zero on the present time scale of ~500 ps. For temperatures $T > 220$

Table 2. Diffusion Constants in Units of 10^{-5} cm^2/s Calculated Using the Einstein Relation for TIP3P, TIP4P, and TIP5P from a 30 Å Cubic Water Box with the Same Electrostatic Treatment As in the Protein Simulation

T/K	TIP3P			TIP4P			TIP5P		
150	0.0018	±	0.0000	0.0018	±	0.0002	0.0007	±	0.0001
160	0.0043	±	0.0002	0.0016	±	0.0002	0.0007	±	0.0002
170	0.0171	±	0.0007	0.0025	±	0.0002	0.0009	±	0.0001
180	0.0444	±	0.0033	0.0036	±	0.0001	0.0009	±	0.0000
190	0.116	±	0.0045	0.0086	±	0.0011	0.0009	±	0.0001
200	0.3104	±	0.0075	0.0193	±	0.0004	0.0014	±	0.0000
210	0.5058	±	0.0146	0.04	±	0.0007	0.0028	±	0.0004
220	0.8463	±	0.0032	0.1306	±	0.0026	0.003	±	0.0001
230	1.243	±	0.0177	0.2699	±	0.0010	0.0073	±	0.0016
240	1.7191	±	0.0464	0.4948	±	0.0044	0.0202	±	0.0002
250	2.3816	±	0.0269	0.8021	±	0.0017	0.0459	±	0.0072
260	2.8328	±	0.0261	1.1895	±	0.0040	0.2601	±	0.0001
280	3.9614	±	0.1640	2.1882	±	0.0674	1.1849	±	0.0100
300	5.4596	±	0.0158	3.595	±	0.0581	2.8162	±	0.0190

K (above the dynamical transition temperature), $C(t)$ decays rapidly (<50 ps) to ~0.5, but the decay is much slower at lower T.

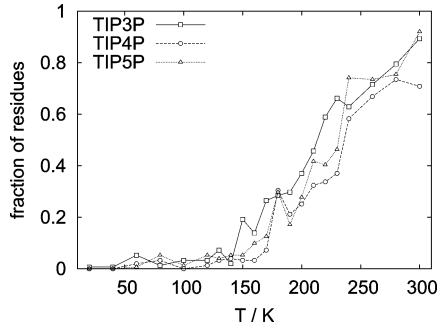

Figure 5. Fraction of residues exhibiting anharmonic dynamics.

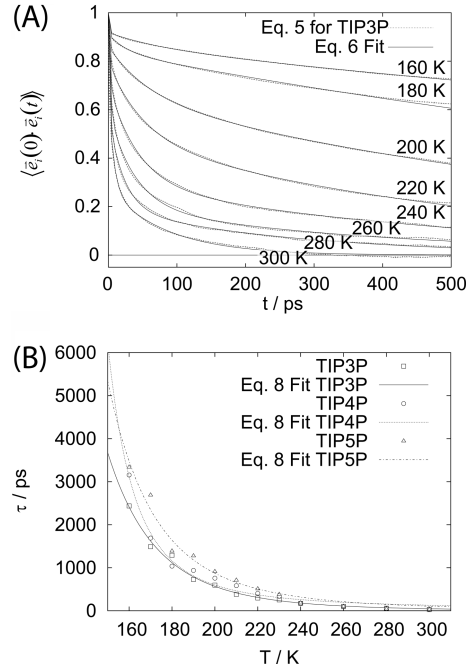

Figure 6. (A) Protein hydration water dipole orientational autocorrelation functions (eq 5) for TIP3P and eq 6 fitted to data from eq 5. TIP4P and TIP5P data are similar. (B) Reorientational relaxation lifetimes τ (eq 7) fitted with the Vogel−Fulcher−Tammann equation (eq 8).

There is good agreement between the fitted curves of eq 6 and the data (Figure 6A). Figure 7 and Table 3 present the temperature dependence of the resulting fitted parameters. At low T ($\leq$ 180 K), the process associated with relaxation time τ_2 dominates, with a weight factor, $1 - a_0 - a_1 \approx 1$. A decrease of $1 - a_0 - a_1$ (i.e., an increase of a_0 and/or a_1) is observed for $T > 180$ K, indicating the activation of additional relaxation processes. For $T \geq 240$ K, the three components are approximately equally weighted.

The temperature dependences of the weights and values of τ_0 and τ_1 behave very similarly to each other, with the weight of the τ_1 component being larger and the values being ~10 times larger than τ_0. τ_0 and τ_1 have broad maxima at ~260 and 210 K, respectively. For temperatures $T \leq 180$ K, the τ_1 component jumps to high values, accompanied by a drop in its weight.

The relaxation times τ, derived by eq 7, are given in Figure 6B. Relaxation times at 300 K from the full sets of simulations at this temperature are 31 ± 3, 35 ± 3, and 32 ± 6 ps for TIP3P, TIP4P, and TIP5P, respectively, and rise by 2 orders of magnitude as the temperature decreases to 160 K.

At temperatures $T > T^*$, glass-forming liquids exhibit an Arrhenius relaxation mechanism $\tau \propto \exp(-E_\beta/k_B T)$ due to the behavior of the β relaxation which, at T^*, splits into a fast β relaxation and a slow α relaxation.[112,113] The α relaxation may often be described with a Vogel−Fulcher−Tammann (VFT) equation over the range $T_g < T < T^*$, i.e.,

$$\tau(T) = \tau_c \exp\left(\frac{A}{T - T_0}\right) \tag{8}$$

with fitting parameters τ_c, A, and T_0. Cooperativity of β-relaxation events has been suggested as the origin of the α relaxation. A similar VFT relationship between τ and T has been used in glass physics,[112] where T_0 has been hypothesized to be the Kauzmann temperature and $A = (E_\beta/R)[(T^* - T_0)/T^*]$ with E_β as the activation energy for the β relaxations. The Kauzmann temperature is the temperature at which the entropies of the supercooled liquid and the corresponding crystal are in principle equal.[113,114]

Angell proposed a "fragile-to-strong" classification of liquids in which relaxation times of "strong" liquids follow

an Arrhenius trend (e.g., SiO_2), whereas "fragile" liquids deviate from such a behavior.[115] The VFT relation describes well the present data for $T > 160$ K, although the fitted parameter values were subject to large errors, thus classifying the protein hydration shell water as a "fragile" liquid in Angell's scheme.

3.5. Local Orientational Ordering. The local orientational ordering of water dipoles can be quantified by the distance-dependent Kirkwood G factor, defined as follows:[116]

$$G_{K,h}(r) = \langle \vec{\mu}_i \cdot \vec{M}(r) \rangle \tag{9}$$

with

$$\vec{M}(r) = \sum_{r_{ij} \le r} \vec{\mu}_j \tag{10}$$

where $\vec{\mu}_i$ denotes a unit vector in the direction of the dipole moment of molecule i. $G_{K,h}(r)$ is equal to two if a pair of water dipoles is parallel. Elevated $G_{K,h}(r)$ therefore corresponds to high angular correlations between water molecules.

Figure 8 shows $G^{r_{max}\pm0.2}_{K,h}(T)$, as a function of temperature for different water models, averaged over 0.2 Å around r_{max}, where r_{max} is the most probable near neighbor distance, taken to be equal to the position of the first peak in the water oxygen−oxygen radial distribution function $g_{OO}(r)$ (∼2.8 Å). Other simulation studies obtained similar values for $G^{r_{max}}_{K,h}(T)$ at ∼2.8 Å and 300 K.[117,118]

A systematic decrease in $G^{r_{max}\pm0.2}_{K,h}(T)$ is evident above 200 K for all water models in the hydration layer of myoglobin (in the hydrated power model), associated with the increased diffusion (see Figure 3B). Although $G^{r_{max}\pm0.2}_{K,h}(T)$ obtained for a myoglobin solution is slightly higher than that of the hydrated powder model, the temperature dependence of $G^{r_{max}\pm0.2}_{K,h}(T)$ shows a similar trend to that of the hydrated powder model. The observed higher values of $G^{r_{max}\pm0.2}_{K,h}(T)$ in myoglobin solution can be attributed to the fact that all the water molecules (both bulk and interfacial) have complete first coordination shells in solution, while in the powder model some can have partial coordination shells. The results reported in Figures 3A,B and 8 are consistent with dynamical coupling between the protein and the solvent since the transition consistently occurs at ∼220 K, captured by all TIP water models investigated here.

4. Conclusions

The effect of the variation of the water model on the temperature dependence of protein and hydration water dynamics has been investigated here by performing molecular dynamics simulations of hydrated myoglobin. Both protein and water properties were analyzed, including the time-averaged structures of the protein, the average mean-square displacements of the protein and water atoms, the solvent reorientational relaxation times, and pair angular correlations between the water molecules.

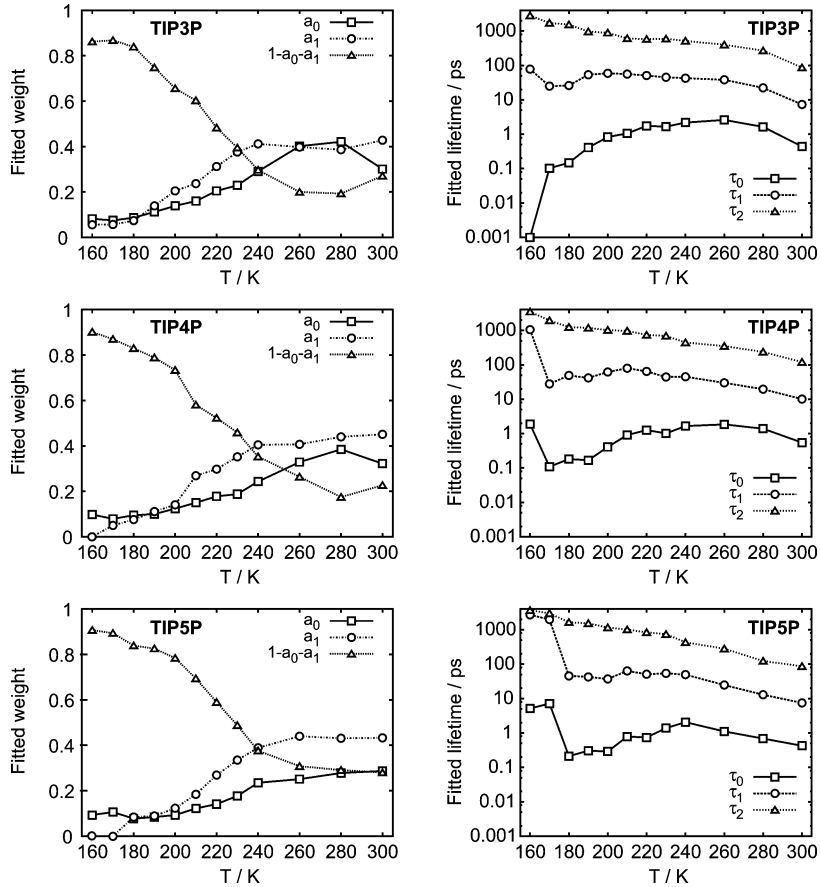

Figure 7. Fitted parameter values a_0, a_1, $1 - a_0 - a_1$, τ_0, τ_1, and τ_2 from eq 6. Lines connect points as a guide to the eye. Numerical values are given in Table 3.

Table 3. Fitted Parameter Values for eq 6[a]

	T/K	TIP3P	TIP4P	TIP5P		T/K	TIP3P	TIP4P	TIP5P
	160	0.08	0.10	0.09		160	0.00	1.88	5.11
	170	0.08	0.08	0.11		170	0.10	0.11	7.15
	180	0.09	0.09	0.08		180	0.15	0.18	0.21
	190	0.11	0.10	0.08		190	0.41	0.17	0.31
	200	0.14	0.12	0.09		200	0.83	0.41	0.29
	210	0.16	0.15	0.12		210	1.06	0.91	0.78
a_0	220	0.21	0.18	0.14	τ_0	220	1.74	1.26	0.74
	230	0.23	0.19	0.18		230	1.66	1.01	1.38
	240	0.29	0.24	0.24		240	2.18	1.66	2.06
	260	0.40	0.33	0.25		260	2.60	1.85	1.11
	280	0.42	0.38	0.28		280	1.63	1.39	0.69
	300	0.30	0.32	0.29		300	0.44	0.55	0.43
	160	0.06	0.00	0.00		160	78.22	1049.77	2710.67
	170	0.06	0.05	0.00		170	25.05	27.77	1984.47
	180	0.07	0.08	0.08		180	26.10	48.92	45.39
	190	0.14	0.11	0.09		190	53.70	41.52	42.55
	200	0.20	0.14	0.12		200	59.20	61.70	37.20
	210	0.24	0.27	0.18		210	56.04	79.61	63.44
a_1	220	0.31	0.30	0.27	τ_1	220	50.97	64.38	51.01
	230	0.38	0.35	0.33		230	45.34	44.00	53.98
	240	0.41	0.40	0.39		240	42.57	44.90	49.49
	260	0.40	0.41	0.44		260	38.17	29.87	24.68
	280	0.39	0.44	0.43		280	22.27	19.51	12.89
	300	0.43	0.45	0.43		300	7.32	10.09	7.46
	160	0.86	0.90	0.91		160	2819.49	3498.03	3679.43
	170	0.87	0.87	0.89		170	1714.96	1939.45	3007.36
	180	0.84	0.83	0.84		180	1535.37	1245.80	1650.42
	190	0.75	0.79	0.83		190	963.95	1182.51	1538.97
	200	0.66	0.73	0.78		200	890.55	1020.11	1156.62
	210	0.60	0.58	0.69		210	610.75	968.10	1007.51
$1 - a_0 - a_1$	220	0.48	0.52	0.59	τ_2	220	580.03	736.41	838.47
	230	0.40	0.46	0.49		230	594.33	690.84	741.91
	240	0.30	0.35	0.38		240	515.06	443.10	431.47
	260	0.20	0.26	0.31		260	398.39	349.69	280.67
	280	0.19	0.18	0.29		280	269.09	235.99	123.27
	300	0.27	0.23	0.28		300	86.83	119.99	86.76

[a] τ_1, τ_2, and τ_3 in ps.

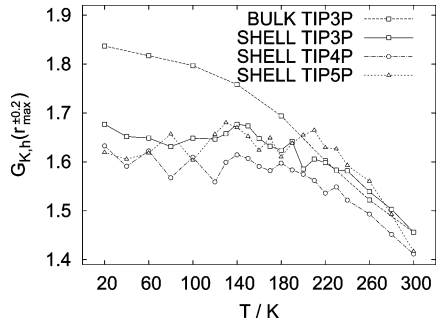

Figure 8. Local orientational ordering of water dipoles measured with the distance-dependent Kirkwood *G*-factor $G^{r_{max}\pm 0.2}_{K,h}(T)$ averaged over 0.2 Å around the maximum of the oxygen−oxygen radial distribution function as a function of temperature for different water models in the hydration shell ("SHELL") and for "BULK" TIP3P. $G^{r_{max}\pm 0.2}_{K,h}(T)$ for "BULK" TIP3P is scaled by $c = 0.89$ (see text). Lines connect points as a guide to the eye.

Variation of the water model between TIP3P, TIP4P, and TIP5P leads to the same time-averaged structures of the protein to within statistical error. Also, for all three water models, the temperature-dependent mean-square displacement exhibits the well-known dynamical transition at $T_g \approx 220$ K. Furthermore, it has been previously shown that the SPC/E water model[119] with the GROMOS protein force field[120] also reproduces the T_g protein dynamical transition at the same temperature.[103]

Mid-infrared pump−probe spectroscopy on the dynamics of HDO in H_2O yielded an orientational lifetime of $\tau_{PP} = 2.5$ ps for bulk water and $\tau_{PP} > 10$ ps for "immobilized" water in the solvation shell of tetramethylurea,[33,121] which corresponds to a retardation factor of at least 4. The bulk water relaxation time τ_D was derived to be 8.8 ps from molecular dynamics studies and 7 ps from experiments on dielectric relaxation, both at 303 K.[122] [Pump−probe experiments measure different lifetimes than dielectric relaxation experiments or the present simulation data: whereas the lifetime τ_{PP} from pump−probe experiments is related to the second-order correlation function $\langle P_2(\cos\theta(t))\rangle$ (where P_2 is the second-order Legendre polynomial), the lifetimes τ_D from dielectric relaxation and the present work are determined by the first-order correlation function $\langle P_1(\cos\theta(t))\rangle$. The ratio between τ_{PP} and τ_D depends on the details of molecular diffusion: $\tau_{PP} = 3\tau_D$ for simple rotational diffusion but is different for other types of dynamics.[123]]

Experiments and simulations have shown that the reorientational dynamics of protein hydration water is slowed down relative to the bulk, e.g.,[5,26,27,34,36,40] with the slowing down being influenced by heterogeneous surface roughness and charge distribution.[21,24,39,40,111]

A recent measurement of cell water dynamics estimates the rotational correlation time for water directly interacting with biomolecular surfaces to be 27 ps.[14] The present protein hydration water relaxation times at 300 K are 31 ± 3, 35 ± 3, and 32 ± 6 ps for TIP3P, TIP4P, and TIP5P, respectively. These times are very similar to each other and to the values in ref 14 and are approximately a factor of 4 slower then the bulk relaxation times measured in ref 122.

A decrease in the pair angular correlations between water molecules in the protein hydration layer, calculated using the Kirkwood *G* factor, accompanies the dynamical transition.

Taken together, the present results suggest that the global dynamical properties of the protein and hydration water are not significantly affected by variation of the water models among TIP3P, TIP4P, and TIP5P. Although these models have documented different bulk phase properties, they behave similarly on the protein surface for the quantities investigated.

Broadly speaking, the present work has served two purposes. First, the relative invariance of the simulation-derived temperature-dependent protein and water dynamics to the water potential used bolsters the argument for the reliability of the simulation analyses of these phenomena previously published using only one water potential.[8,9,41−43,48,57,68−70,77,86,96,124−127] Second, the results indicate that, although general interchangeability of water potentials in protein simulations is not expected and cannot be assumed, for some purposes at least it is safe to choose between TIP3P, TIP4P, and TIP5P as the water potential used in protein simulations with CHARMM.

Acknowledgment. This work was funded by a U.S. Department of Energy Laboratory—Directed Research and Development grant.

References

(1) Finney, J. L. *J. Mol. Liq.* **2001**, *90*, 303–312.

(2) Chaplin, M. *Nat. Rev. Mol. Cell Biol.* **2006**, *7*, 861–866.

(3) Kauzmann, W. *Adv. Protein Chem.* **1959**, *14*, 1–63.

(4) Dill, K. *Biochemistry* **1990**, *29*, 7133–7155.

(5) Halle, B. *Philos. Trans. R. Soc. London, Ser. B* **2004**, *359*, 1207–1224.

(6) Paciaroni, A.; Cinelli, S.; Cornicchi, E.; Francesco, A.; Onori, G. *Chem. Phys. Lett.* **2005**, *410*, 400–403.

(7) Nakasako, M. *Philos. Trans. R. Soc. London, Ser. B* **2004**, *359*, 1191–1206.

(8) Oleinikova, A.; Smolin, N.; Brovchenko, I.; Geiger, A.; Winter, R. *J. Phys. Chem. B* **2005**, *109*, 1988–1998.

(9) Smolin, N.; Oleinikova, A.; Brovchenko, I.; Geiger, A.; Winter, R. *J. Phys. Chem. B* **2005**, *109*, 10995–11005.

(10) Zanotti, J. M.; Bellissent-Funel, M. C.; Parello, J. *Biophys. J.* **1999**, *76*, 2390–2411.

(11) Williams, M. A.; Goodfellow, J. M.; Thornton, J. M. *Protein Sci.* **1994**, *3*, 1224–1235.

(12) Denisov, V. P.; Halle, B. *Faraday Discuss.* **1996**, *103*, 227–244.

(13) Stadler, A. M.; Embs, J. P.; Digel, I.; Artmann, G. M.; Unruh, T. B.

(14) Persson, E.; Halle, B. *Proc. Natl. Acad. Sci. U.S.A.* **2008**, *105*, 6266–6271.

(15) Svergun, D. I.; Richard, S.; Koch, M. H. J.; Sayers, Z.; Kuprin, S.; Zaccai, G. *Proc. Natl. Acad. Sci. U.S.A.* **1998**, *95*, 2267–2272.

(16) Merzel, F.; Smith, J. C. *Proc. Natl. Acad. Sci. U.S.A.* **2002**, *99*, 5378–5383.

(17) Merzel, F.; Smith, J. C. *J. Chem. Inf. Model.* **2005**, *45*, 1593–1599.

(18) Zanotti, J. M.; Bellissent-Funel, M. C.; Chen, S. H. *Phys. Rev. E* **1999**, *59*, 3084–3093.

(19) Bellissent-Funel, M. C.; Chen, S. H.; Zanotti, J. M. *Phys. Rev. E* **1995**, *51*, 4558–4569.

(20) Dellerue, S.; Bellissent-Funel, M. C. *Chem. Phys.* **2000**, *258*, 315–325.

(21) Russo, D.; Hura, G.; Head-Gordon, T. *Biophys. J.* **2004**, *86*, 1852–1862.

(22) Takahara, S.; Sumiyama, N.; Kittaka, S.; Yamaguchi, T.; Bellissent-Funel, M. *J. Phys. Chem. B* **2005**, *109*, 11231–11239.

(23) Jansson, H.; Bergman, R.; Swenson, J. *J. Non-Cryst. Solids* **2006**, *352*, 4410–4416.

(24) Malardier-Jugroot, C.; Johnson, M. E.; Murarka, R. K.; Head-Gordon, T. *Phys. Chem. Chem. Phys.* **2008**, *10*, 4903–4908.

(25) Frölich, A.; Gabel, F.; Jasnin, M.; Lehnert, U.; Österhelt, D.; Stadler, A. M.; Tehei, M.; Weik, M.; Wood, K.; Zaccai, G. *Faraday Discuss.* **2009**, *141*, 117–130.

(26) Halle, B.; Andersson, T.; Forsen, S.; Lindman, B. *J. Am. Chem. Soc.* **1981**, *103*, 500–508.

(27) Polnaszek, C. F.; Bryant, R. G. *J. Chem. Phys.* **1984**, *81*, 4038–4045.

(28) Polnaszek, C. F.; Bryant, R. G. *J. Am. Chem. Soc.* **1984**, *106*, 428–429.

(29) Polnaszek, C. F.; Hanggi, D. A.; Carr, P. W.; Bryant, R. G. *Anal. Chim. Acta* **1987**, *194*, 311–315.

(30) Carlstrom, G.; Halle, B. *Langmuir* **1988**, *4*, 1346–1352.

(31) Armstrong, B. D.; Han, S. *J. Am. Chem. Soc.* **2009**, *131*, 4641–4647.

(32) Pal, S. K.; Peon, J.; Zewail, A. H. *Proc. Natl. Acad. Sci. U.S.A.* **2002**, *99*, 1763–1768.

(33) Rezus, Y. L. A.; Bakker, H. J. *J. Phys. Chem. A* **2008**, *112*, 2355–2361.

(34) Lee, S. H.; Rossky, P. J. *J. Chem. Phys.* **1994**, *100*, 3334–3345.

(35) Bizzarri, A. R.; Cannistraro, S. *Phys. Rev. E* **1996**, *53*, R3040–R3043.

(36) Rocchi, C.; Bizzarri, A.; Cannistraro, S. *Phys. Rev. E* **1998**, *57*, 3315–3325.

(37) Bizzarri, A. R.; Cannistraro, S. *J. Phys. Chem. B* **2002**, *106*, 6617–6633.

(38) Marchi, M.; Sterpone, F.; Ceccarelli, M. *J. Am. Chem. Soc.* **2002**, *124*, 6787–6791.

(39) Argyris, D.; Tummala, N. R.; Striolo, A.; Cole, D. R. *J. Phys. Chem. C* **2008**, *112*, 13587–13599.

(40) Johnson, M. E.; Malardier-Jugroot, C.; Murarka, R. K.; Head-Gordon, T. *The J. Phys. Chem. B* **2008**, *113*, 4082–4092.

(41) MacKerell, A. D.; et al. *J. Phys. Chem. B* **1998**, *102*, 3586–3616.

(42) Brooks, B. R.; Bruccoleri, R. E.; Olafson, B. D.; States, D. J.; Swaminathan, S.; Karplus, M. *J. Comput. Chem.* **1982**, *4*, 187–217.

(43) MacKerell, A.; Kuczera, J. W.; Karplus, M. *J. Am. Chem. Soc.* **1995**, *117*, 11946–11975.

(44) Pearlman, D. A.; Case, D. A.; Caldwell, J. W.; Ross, W. S.; Cheatharm, T. E., III; De Bolt, S.; Ferguson, D.; Seibel, G.; Kollmann, P. *Comput. Phys. Commun.* **1995**, *91*, 1–41.

(45) Scott, W. R. P.; Hünenberg, P. H.; Tironi, I. G.; Mark, A. E.; Billeter, S. R.; Fennen, J.; Torda, A. E.; Huber, T.; Krüger, P.; van Gunsteren, W. F. *J. Phys. Chem. A* **1999**, *103*, 3596–3607.

(46) Jorgensen, W. L.; Maxwell, D. S.; Tirado-Rives, J. *J. Am. Chem. Soc.* **1996**, *118*, 11225–11236.

(47) Guillot, B. *J. Mol. Liq.* **2002**, *101*, 219–260.

(48) Nutt, D. R.; Smith, J. C. *J. Am. Chem. Soc.* **2008**, *130*, 13066–13073.

(49) Cui, J.; Battle, K.; Wierzbicki, A.; Madura, J. D. *Int. J. Quantum Chem.* **2009**, *109*, 73−80; 16th Conference on Current Trends in Computational Chemistry, Jackson, MS, Nov. 2−3, 2007.

(50) Mahoney, M. W.; Jorgensen, W. L. *J. Chem. Phys.* **2000**, *112*, 8910–8922.

(51) Nandi, N.; Bagchi, B. *J. Phys. Chem. B* **1997**, *101*, 10954–10961.

(52) Vega, C.; Abascal, J. L. F.; Conde, M. M.; Aragones, J. L. *Faraday Discuss.* **2009**, *141*, 251–276.

(53) Kwac, K.; Lee, K. K.; Han, J. B.; Cho, M. *J. Chem. Phys.* **2008**, *128*, 105106.

(54) Shirts, M. R.; Pande, V. S. *J. Chem. Phys.* **2005**, *122*, 134508–134508.

(55) van der Spoel, D.; Lindahl, E. *J. Phys. Chem. B* **2003**, *107*, 11178–11187.

(56) Mark, P.; Nilsson, L. *J. Phys. Chem. B* **2001**, *105*, 8028–8035.

(57) Nutt, D. R.; Smith, J. C. *J. Chem. Theory Comput.* **2007**, *3*, 1550–1560.

(58) Jorgensen, W. L.; Chandrasekhar, J.; Madura, J. D.; Impey, R. W.; Klein, M. L. *J. Chem. Phys.* **1983**, *79*, 926–935.

(59) Parak, F. G.; Formanek, H. *Acta Crystallogr., Sect. A* **1971**, *27*, 573–578.

(60) Knapp, E. W.; Fischer, S. F.; Parak, F. *J. Phys. Chem.* **1982**, *86*, 5042–5047.

(61) Parak, F.; Knapp, E. W. *Proc. Natl. Acad. Sci. U.S.A.* **1984**, *81*, 7088–7092.

(62) Doster, W.; Cusack, S.; Petry, W. *Nature* **1989**, *337*, 754–756.

(63) Smith, J. C. *Q. Rev. Biophys.* **1991**, *24*, 227–291.

(64) Rasmussen, B. F.; Stock, A. M.; Ringe, D.; Petsko, G. A. *Nature* **1992**, *357*, 423–424.

(65) Fitter, J.; Lechner, R. E.; Dencher, N. A. *Biophys. J.* **1997**, *73*, 2126–2137.

(66) Ostermann, A.; Waschipky, R.; Parak, F. G.; Nienhaus, G. U. *Nature* **2000**, *404*, 205–208.

(67) Ringe, D.; Petsko, G. A. *Biophys. Chem.* **2003**, *105*, 667–680.

(68) Tournier, A. L.; Xu, J.; Smith, J. C. *Biophys. J.* **2003**, *85*, 1871–1875.

(69) Tournier, A. L.; Smith, J. C. *Phys. Rev. Lett.* **2003**, *91*, 208106.

(70) Schulz, R.; Krishnan, M.; Daidone, I.; Smith, J. C. *Biophys. J.* **2009**, *96*, 476–484.

(71) Roh, J. H.; Curtis, J. E.; Azzam, S.; Novikov, V. N.; Peral, I.; Chowdhuri, Z.; Gregory, R. B.; Sokolov, A. P. *Biophys. J.* **2006**, *91*, 2573–2588.

(72) Iben, I. E. T.; Braunstein, D.; Doster, W.; Frauenfelder, H.; Hong, M. K.; Johnson, J. B.; Luck, S.; Ormos, P.; Schulte, A.; Steinbach, P. J.; Xie, A. H.; Young, R. D. *Phys. Rev. Lett.* **1989**, *62*, 1916–1919.

(73) Ferrand, M.; Dianoux, A. J.; Petry, W.; Zaccai, G. *Proc. Natl. Acad. Sci. U.S.A.* **1993**, *90*, 9668–9672.

(74) Fitter, J.; Ernst, O. P.; Hauss, T.; Lechner, R. E.; Hofmann, K. P.; Dencher, N. A. *Eur. Biophys. J.* **1998**, *27*, 638–645.

(75) Fitter, J.; Verclasc, S. A. W.; Lechnerc, R. E.; Seelerta, H.; Dencher, N. A. *FEBS Lett.* **1998**, *433*, 321–325.

(76) Fitter, J. *Biophys. J.* **1999**, *76*, 1034–1042.

(77) Vitkup, D.; Ringe, D.; Petsko, G. A.; Karplus, M. *Nat. Struct. Mol. Biol.* **2000**, *7*, 34–38.

(78) Reat, V.; Dunn, R.; Ferrand, M.; Finney, J. L.; Daniel, R. M.; Smith, J. C. *Proc. Natl. Acad. Sci. U.S.A.* **2000**, *97*, 9961–9966.

(79) Fenimore, P. W.; Frauenfelder, H.; McMahon, B. H.; Parak, F. G. *Proc. Natl. Acad. Sci. U.S.A.* **2002**, *99*, 16047–16051.

(80) Paciaroni, A.; Cinelli, S.; Onori, G. *Biophys. J.* **2002**, *83*, 1157–1164.

(81) Chaplin, M. F. *Biochem. Mol. Biol. Edu.* **2001**, *29*, 54–59.

(82) Lee, A. L.; Wand, A. J. *Nature* **2001**, *411*, 501–504.

(83) Hayward, J. A.; Smith, J. C. *Biophys. J.* **2002**, *82*, 1216–1225.

(84) Roh, J. H.; Novikov, V. N.; Gregory, R. B.; Curtis, J. E.; Chowdhuri, Z.; Sokolov, A. P. *Phys. Rev. Lett.* **2005**, *95*, 038101.

(85) Doster, W.; Settles, M. *Biochim. Biophys. Acta* **2005**, *1749*, 173–186.

(86) Krishnan, M.; Kurkal-Siebert, V.; Smith, J. C. *J. Phys. Chem. B* **2008**, *112*, 5522–5533.

(87) Cordone, L.; Ferrand, M.; Vitrano, E.; Zaccai, G. *Biophys. J.* **1999**, *76*, 1043–1047.

(88) Tsai, A. M.; Neumann, D. A.; Bell, L. N. *Biophys. J.* **2000**, *79*, 2728–2732.

(89) Tarek, M.; Tobias, D. J. *Phys. Rev. Lett.* **2002**, *88*, 138101.

(90) Ding, X.; Rasmussen, B. F.; Petsko, G. A.; Ringe, D. *Biochemistry* **1994**, *33*, 9285–9293.

(91) Parak, F. G.; Frolov, E. N.; Kononenko, A. A.; Mössbauer, R. L.; Goldanskii, V. I.; Rubin, A. B. *FEBS Lett.* **1980**, *117*, 368–372.

(92) Daniel, R. M.; Smith, J. C.; Ferrand, M.; Hery, S.; Dunn, R.; Finney, J. L. *Biophys. J.* **1998**, *75*, 2504–2507.

(93) Dunn, R.; Reat, V.; Finney, J. L.; Ferrand, M.; Smith, J. C.; Daniel, R. M. *Biochem. J.* **2000**, *346*, 355–358.

(94) Bragger, J. M.; Dunn, R. V.; Daniel, R. M. *Biochim. Biophys. Acta* **2000**, *1480*, 278–282.

(95) Kurkal, V.; Daniel, R. M.; Finney, J. L.; Tehei, M.; Dunn, R. V.; Smith, J. C. *Biophys. J.* **2005**, *89*, 1282–1287.

(96) Neria, E.; Fischer, S.; Karplus, M. *J. Chem. Phys.* **1996**, *105*, 1902–1921.

(97) Mark, P.; Nilsson, L. *J. Phys. Chem. A* **2001**, *105*, 9954–9960.

(98) Vojtechovsky, J.; Chu, K.; Berendzen, J.; Sweet, R. M.; Schlichting, I. *Biophys. J.* **1999**, *77*, 2153–2174.

(99) Ryckaert, J. P.; Ciccotti, G.; Berendsen, H. J. C. *J. Comp. Phys.* **1977**, *23*, 321–341.

(100) Berendsen, H. J. C.; Postma, J. P. M.; van Gunsteren, W. F.; DiNola, A.; Haak, J. R. *J. Chem. Phys.* **1984**, *81*, 3684–3690.

(101) Hess, B.; Kutzner, C.; van der Spoel, D.; Lindahl, E. *J. Chem. Theory Comput.* **2008**, *4*, 435–447.

(102) Phillips, J. C.; Braun, R.; Wang, W.; Gumbart, J.; Tajkhorshid, E.; Villa, E.; Chipot, C.; Skeel, R. D.; Kale, L.; Schulten, K. *J. Comput. Chem.* **2005**, *26*, 1781–1802.

(103) Wong, C. F.; Zheng, C.; Mccammon, J. A. *Chem. Phys. Lett.* **1989**, *154*, 151–154.

(104) Arcangeli, C.; Bizzarri, A. R.; Cannistraro, S. *Chem. Phys. Lett.* **1998**, *291*, 7–14.

(105) Parak, F. G.; Knapp, E. W.; Kucheida, D. *J. Mol. Biol.* **1982**, *161*, 177–194.

(106) Tarek, M.; Tobias, D. J. *Biophys. J.* **2000**, *79*, 3244–3257.

(107) Steinbach, P.; Brooks, B. *Proc. Natl. Acad. Sci. U.S.A.* **1993**, *90*, 9135–9139.

(108) Teeter, M. M.; Yamano, A.; Stec, B.; Mohanty, U. *Proc. Natl. Acad. Sci. U. S. A.* **2001**, *98*, 11242.

(109) Caliskan, G.; Kisliuk, A.; Sokolov, A. P. *J. Non-Cryst. Solids* **2002**, *307*−*310*, 868–873.

(110) van der Spoel, D.; van Maaren, P. J. *J. Chem. Theory Comput.* **2006**, *2*, 1–11.

(111) Murarka, R. K.; Head-Gordon, T. *J. Chem. Phys.* **2007**, *126*, 215101.

(112) Rault, J. *J. Non-Cryst. Solids* **2000**, *271*, 177–217.

(113) Debenedetti, P. G.; Stillinger, F. H. *Nature* **2001**, *410*, 259–267.

(114) Kauzmann, W. *Chem. Rev.* **1948**, *43*, 219–256.

(115) Angell, C. A. *Science* **1995**, *267*, 1924–1935.

(116) Kirkwood, J. G. *J. Chem. Phys.* **1939**, *7*, 911–919.

(117) Boresch, S.; Ringhofer, S.; Höechtl, P.; Steinhauser, O. *Biophys. Chem.* **1999**, *78*, 43–68.

(118) Höechtl, P.; Boresch, S.; Bitomsky, W.; Steinhauser, O. *J. Chem. Phys.* **1998**, *109*, 4927–4937.

(119) Berendsen, H. J. C.; Grigera, J. R.; Straatsma, T. P. *J. Phys. Chem.* **1987**, *91*, 6269–6271.

(120) Hermans, J.; Berendsen, H. J. C.; van Gunsteren, W. F.; Postma, J. P. M. *Biopolymers* **1984**, *23*, 1513–1518.

(121) Rezus, Y. L. A.; Bakker, H. J. *J. Chem. Phys.* **2005**, *123*, 114502.

(122) Rϕnne, C.; Thrane, L.; Åstrand, P. O.; Wallqvist, A.; Mikkelsen, K. V.; Keiding, S. R. *J. Chem. Phys.* **1997**, *107*, 5319–5331.

(123) Laage, D.; Hynes, J. T. *Science* **2006**, *311*, 832–835.

(124) McCammon, J. A.; Gelin, B. R.; Karplus, M. *Nature* **1977**, *267*, 585–590.

(125) Karplus, M.; Kushick, J. N. *Macromolecules* **1981**, *14*, 325–332.

(126) Smith, J. C.; Kuczera, K.; Karplus, M. *Proc. Natl. Acad. Sci. U.S.A.* **1990**, *87*, 1601–1605.

(127) Setny, P.; Wang, Z.; Cheng, L. T.; Li, B.; McCammon, J. A.; Dzubiella, J. *Phys. Rev. Lett.* **2009**, *103*, 187801.

CT9006508